Available online at www.sciencedirect.com
ScienceDirect
Solid State Ionics 177 (2006) 1509–1516
SOLID STATE IONICS
www.elsevier.com/locate/ssi

The studies on structural and thermal properties of delithiated $Li_xNi_{1/3}Co_{1/3}Mn_{1/3}O_2$ ($0<x\leq 1$) as a cathode material in lithium ion batteries

J. Li, Z.R. Zhang, X.J. Guo, Y. Yang *

State Key Lab for Physical Chemistry of Solid Surface, Department of Chemistry, Xiamen University, Xiamen 361005, China

Received 26 December 2005; received in revised form 10 March 2006; accepted 17 March 2006

Abstract

The structural and thermal properties of the delithiated $Li_xNi_{1/3}Co_{1/3}Mn_{1/3}O_2$ ($0<x\leq 1$) material have been investigated by using diffraction and thermoanalytical techniques such as XRD and TG-DSC methods. XRD result shows that the delithiated materials maintain the O3-type structure with defined stoichiometric number at the range of $0.24<x\leq 1$, exhibiting good crystal structural stability. The cobalt and nickel ions in the delithiated materials change their valence state (i.e. Co^{3+} to Co^{4+} and Ni^{3+} to Ni^{4+}) when $x<0.49$; the irreversible changes of the transformation may affect the first cycle of charge–discharge efficiency of the materials. A comparison of the results of TG-DSC with TPD-MS shows that the irreversible change of oxygen species during the delithiation process of $Li_xNi_{1/3}Co_{1/3}Mn_{1/3}O_2$ have great influence on the structural and thermal stability and reversibility of the materials.

Keywords: $Li_xNi_{1/3}Co_{1/3}Mn_{1/3}O_2$ ($0<x\leq 1$); First irreversible capacity loss; Thermal properties; Lithium ion batteries

1. Introduction

Recently, $Li_xNi_{1/3}Mn_{1/3}Co_{1/3}O_2$ has become one of the promising electrode material systems for its high capacity and stable cyclic performance since it was firstly synthesized by Ohzuku and Makimura [1]. It was reported that the material delivers a capacity of ~ 200 mAh/g at the first discharge experiment with a current rate of 0.1 C in a voltage range of 2.5–4.6 V at room temperature [2]. In addition, when cycled between 2.9 and 4.1 V at 1.5 C rate, the material does not show any sign of capacity fade up to 100 cycles, whereas at 5 C rate, a loss of only 18% of capacity is observed after 200 cycles [3]. Different methods have been used to synthesize this kind of material, such as mixed hydroxide method [2–6], sol–gel method [7] and spray pyrolysis method [8,9]. The initial material has an α-$NaFeO_2$-triangular lattice of R-3 m space group with [v3 × v3]R30°-type superlattice structure [10,11]. The original oxidation states for Ni, Co and Mn are +2, +3 and +4 [12], but could change differently in bulk and surface for charging process [13]. In the recent years, anion-substituted materials such as $LiNi_{1/3}Mn_{1/3}Co_{1/3}O_{2-z}F_z$ [14] and lithium-excess materials such as $Li_{1.03}(Ni_{1/3}Mn_{1/3}Co_{1/3})_{0.97}O_2$ [15] were also synthesized to improve its electrochemical performance. In addition, comparing with some commercialized materials, $LiNi_{1/3}Mn_{1/3}Co_{1/3}O_2$ also shows much better thermal stability than their counterpart materials such as $LiCoO_2$ [3].

However, some disadvantages of $LiNi_{1/3}Mn_{1/3}Co_{1/3}O_2$ are also distinctive. For example, quite high irreversible capacity for the material during the first charge–discharge cycle is the most typical one, which will restrict its commercialization [7]. In our previous paper, we have demonstrated that the structural changes of the materials [16] and decomposition of the electrolytes [17] at high anodic potential would bring about irreversible capacity loss in $LiNi_{0.8}Co_{0.2}O_2$ cathode systems. Does similar mechanism exist in $LiNi_{1/3}Mn_{1/3}Co_{1/3}O_2$ material? It should be an interesting subject. Thus, to study the origin of irreversible capacity loss of this system is our main research goal. In this work, we chose one of the effective chemical methods, i.e. use NO_2BF_4 as the oxidant, to quantitatively pull

* Corresponding author. Tel./fax: +86 592 2185753.
E-mail address: yyang@xmu.edu.cn (Y. Yang).

0167-2738/$ - see front matter © 2006 Published by Elsevier B.V.
doi:10.1016/j.ssi.2006.03.055

off some lithium ions from the materials. Then the structural, oxidation state for transition metals and thermal properties of the delithiated materials were characterized and analyzed at different lithium stoichiometric numbers. It is believed that such kind of information will help us to understand the relationship between structure, electrochemical and thermal stability of the materials during an electrochemical process.

2. Experimental

$LiNi_{1/3}Mn_{1/3}Co_{1/3}O_2$ compounds were synthesized by a sol–gel method, with citric acid as a chelating agent as previously reported [18]. Stoichiometric amounts of A.R. purity nickel acetate, cobalt acetate, manganese acetate, and lithium acetate (10% excess) were dissolved into a citric acid solution (the acid-to-metal ion ratio is 1:1). The mixture was stirred at 80 °C for 10 h and then heated at 120 °C for 24 h to form a dry gel. The gel was sintered firstly at 450 °C for 5 h and then at 900 °C for 15 h.

CR2025 coin cells were used to assess the electrochemical properties of the synthesized samples. The cathodes were prepared by mixing 85% of the active material with 10% carbon black and 5% PVDF (wt.%). The cells were assembled with the cathode as prepared, lithium metal as anode, and Celgard 2300 film as separator in an inert-gas box (Labmaster 100, mBraun, Germany). The electrolytes were 1 M $LiPF_6$ dissolved in EC+DMC (1:1 volume ratio) as reported in our previous work [16].

Chemical extraction of lithium from the $LiNi_{1/3}Mn_{1/3}Co_{1/3}O_2$ was carried out by stirring the samples with an acetonitrile solution of NO_2BF_4 as oxidizer for 2 days under argon atmosphere at room temperature, the delithiated reaction is [19]:

$$LiNi_{1/3}Mn_{1/3}Co_{1/3}O_2 + xNO_2BF_4 \rightarrow Li_xNi_{1/3}Mn_{1/3}Co_{1/3}O_2 + xNO_2 + xLiBF_4$$

When the reaction was complete, products were washed to remove $LiBF_4$, then the $Li_xNi_{1/3}Mn_{1/3}Co_{1/3}O_2$ was dried under vacuum at room temperature and stored in glove box to avoid reaction with the moisture.

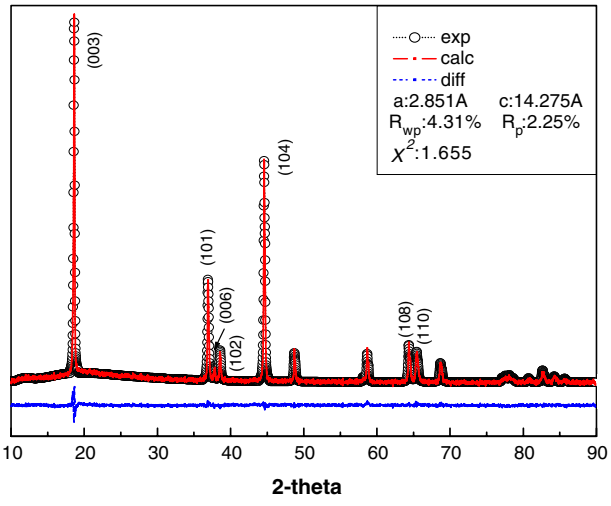

Fig. 1. The experimental, calculated and difference patterns of XRD for $LiNi_{1/3}Mn_{1/3}Co_{1/3}O_2$ material.

Table 1
XRD Rietveld refinement results of cathode material $Li_xNi_{1/3}Mn_{1/3}Co_{1/3}O_2$ ($0<x\leq 1$)

x	a (Å)	c (Å)	c/a	Volume (Å3)	gM	Rwp (%)	Rp (%)	χ2
1	2.851	14.275	5.007	100.479	0.037	4.31	2.55	1.655
0.81	2.850	14.271	5.007	100.397	0.039	3.96	2.32	1.543
0.69	2.835	14.382	5.073	100.100	0.032	2.17	1.78	1.274
0.57	2.825	14.479	5.126	100.054	0.023	2.31	1.74	1.361
0.49	2.822	14.475	5.136	99.950	0.032	1.90	1.51	1.639
0.40	2.822	14.466	5.126	99.776	0.031	2.54	1.68	1.639
0.31	2.822	14.391	5.099	99.278	0.030	2.31	1.74	1.386
0.24	2.822	14.333	5.078	98.867	0.032	2.24	1.60	1.460

gM: the molar content of Ni at the 3a site.

The lithium content was determined by an Inductively Coupled Plasma-Mass method (ICP-MS, HP4500 Hewlett-Packard, USA); average oxidation states of Co, Ni and Mn were determined by iodometric titration. Crystal structure characterization was carried out with X-ray powder diffraction (XRD Panalytical X'pert Philip, Holland) using Cu Kα radiation. The lattice parameters were refined by the Rietveld method with General Structure Analysis Software (GSAS program, Los Alamos National Laboratory, USA). X-ray photoelectron spectroscopy (XPS) of these samples was obtained using Quantum 2000 spectrometer (Physical Electronics, USA) with monochromatic Al-Kα radiation (hí=1486.6 eV) to determine binding energy and valence state of transition metal ions in the materials. Oxygen change and thermostability were carried out with a TG-DSC instrument (Netzsch STA409PC, Germany) and a home built Temperature Programmed Desorption-Mass spectra (TPD-MS) system (the MS spectrometer is Balzersomnistar QMS200).

3. Results and discussion

3.1. Structure and electrochemical performance of $LiNi_{1/3}Co_{1/3}Mn_{1/3}O_2$

In order to make sure the sample synthesized is the target material with a satisfied electrochemical performance, the structure and electrochemical performance of the initial materials were characterized and investigated firstly. Fig. 1 and Table 1 give the Rietveld refinement results of the materials. From Fig. 1, the intensity ratio of (003) and (104) peak is 1.42, and a clear split of (108) and (110) peaks can also be observed, which all suggest an R-3m single phase and minimal disorder in the structure.

For an ideal R-3m crystal, ionic configuration could be regulated as Li at the 3a site (0, 0, 0), M at the 3b site (0, 0, 1/2) and O at the 6c site (0, 0, 1/4) [20]. According to the XPS results shown in Fig. 5, the oxidation states of Ni, Co and Mn in the initial material are proved to be +2, +3 and +4, respectively. In practice, because the ionic radius of Ni^{2+} (r_{Ni2+}=0.70 Å) is similar to that of Li^+ (r^+_{Li}=0.74 Å), it was assumed that a small amount of Ni would go to the 3a Li site. On the other hand, neutron diffraction experiment on the $LiNi_{1-y}Co_yO_2$ [21] and $Li[Ni_xLi_{1/3-2x/3}Mn_{2/3-x/3}]O_2$ [22] system have verified that Co^{3+} and Mn^{4+} do not exist at the 3a Li site. Therefore, a general formula of the cationic distribution as $[Li_{1-z}Ni^{2+}{}_z]_{3a}[Ni^{2+}{}_{1/3-z}Co_{1/3}Mn_{1/3}]_{3b}[O_2]_{6c}$ for $LiNi_{1/3}Co_{1/3}Mn_{1/3}O_2$ material is proposed. The little difference

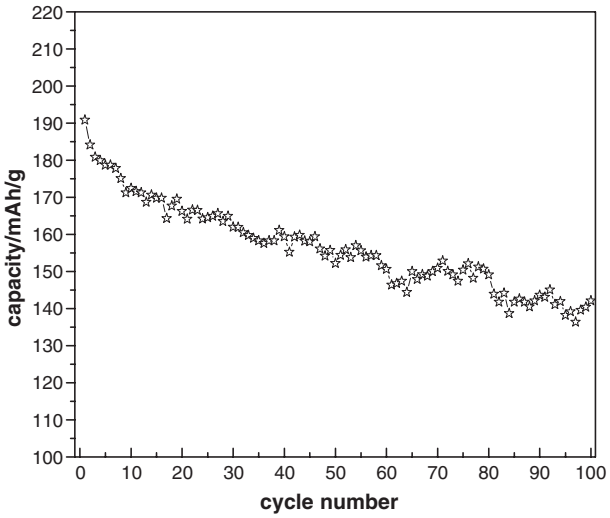

Fig. 2. The cyclic performance of $LiNi_{1/3}Mn_{1/3}Co_{1/3}O_2$ cathode material (0.1 C, 2.0–4.6 V).

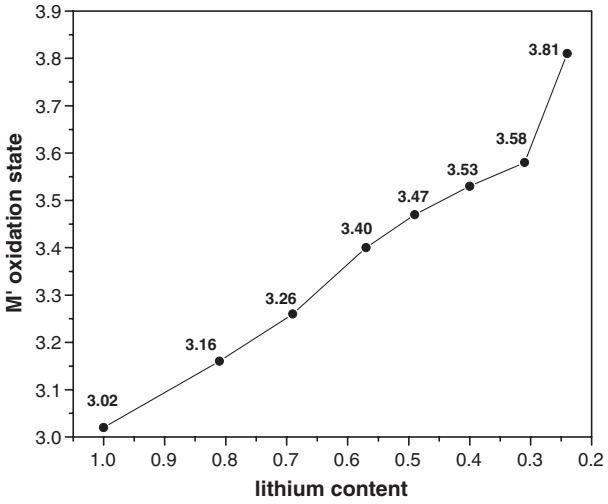

Fig. 4. Average oxidation state of transition metal of $Li_xNi_{1/3}Mn_{1/3}Co_{1/3}O_2$ ($0<x\leq 1$) measured by iodometric titration.

between experimental and calculated patterns and χ^2-factor of 1.655 demonstrated that it is a successful refinement. The hexagonal lattice parameter was determined to be $a=2.850$ (9) Å, $c=14.274(7)$ Å and volume $=100.47(9)$ Å^3, which are consistent with the values reported in the literatures [1–3].

The cyclic performance for $LiNi_{1/3}Co_{1/3}Mn_{1/3}O_2$ material with a current rate of 0.1 C in a voltage range of 2.5–4.6 V at room temperature (~ 25 °C) is shown in Fig. 2. It delivers a capacity of 190.8 mA h/g at first discharge process, fades to 142.1 mA h/g after 100 cycles with capacity retention of 74.5%, exhibiting excellent cyclic performance. However, the irreversible capacity of the materials observed in the first cycle was about 56.7 mA h/g (23%).

3.2. Crystal structure and oxidation state of the delithiated $Li_xNi_{1/3}Co_{1/3}Mn_{1/3}O_2$

In order to understand the different effects of the $LiNi_{1/3}Co_{1/3}Mn_{1/3}O_2$ cathode material on the irreversible capacity during the first charging process, the changes of crystal structure, oxidation state of transition metal ions and oxygen species during the first changing process should be investigated systematically. In the following section, we used a chemical method to prepare delithiated $Li_xNi_{1/3}Co_{1/3}Mn_{1/3}O_2$ samples with different x values, because it can be thought as a similar material with electrochemical delithiation process at different charging potentials without some interference from electrochemical reaction such as the decomposition of the electrolytes. Therefore, the changes of the material at different delithiated stage can be distinguished more clearly and exactly.

Fig. 3 shows the XRD patterns of delithiated $Li_xNi_{1/3}Co_{1/3}Mn_{1/3}O_2$ powder samples. It is shown that the material remains a layered structure for $0.24\leq x\leq 1$ with space group R-3m, but FMHW of the peaks broadens and its intensity also decreases with the decrease of lithium content. These facts indicate that the crystalline structure of the material is weakening as Li ions are released. If we compared the diffraction peaks of (003),

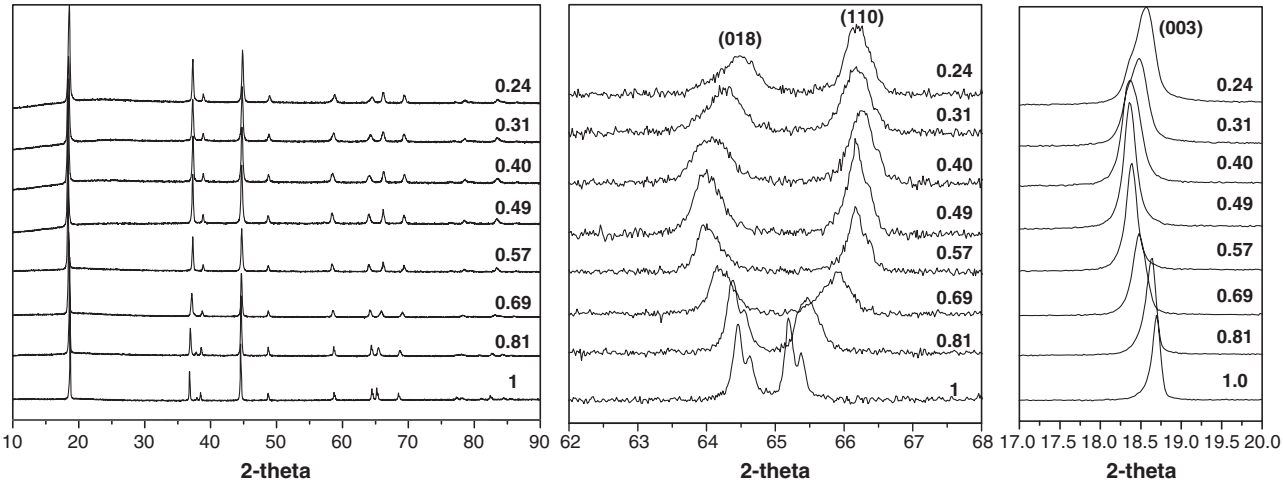

Fig. 3. XRD patterns of $LiNi_{1/3}Mn_{1/3}Co_{1/3}O_2$ ($0<x\leq 1$) cathode materials; the zoom of (108)/(110) and (003) diffraction peaks was also presented at the right of the graph for comparison.

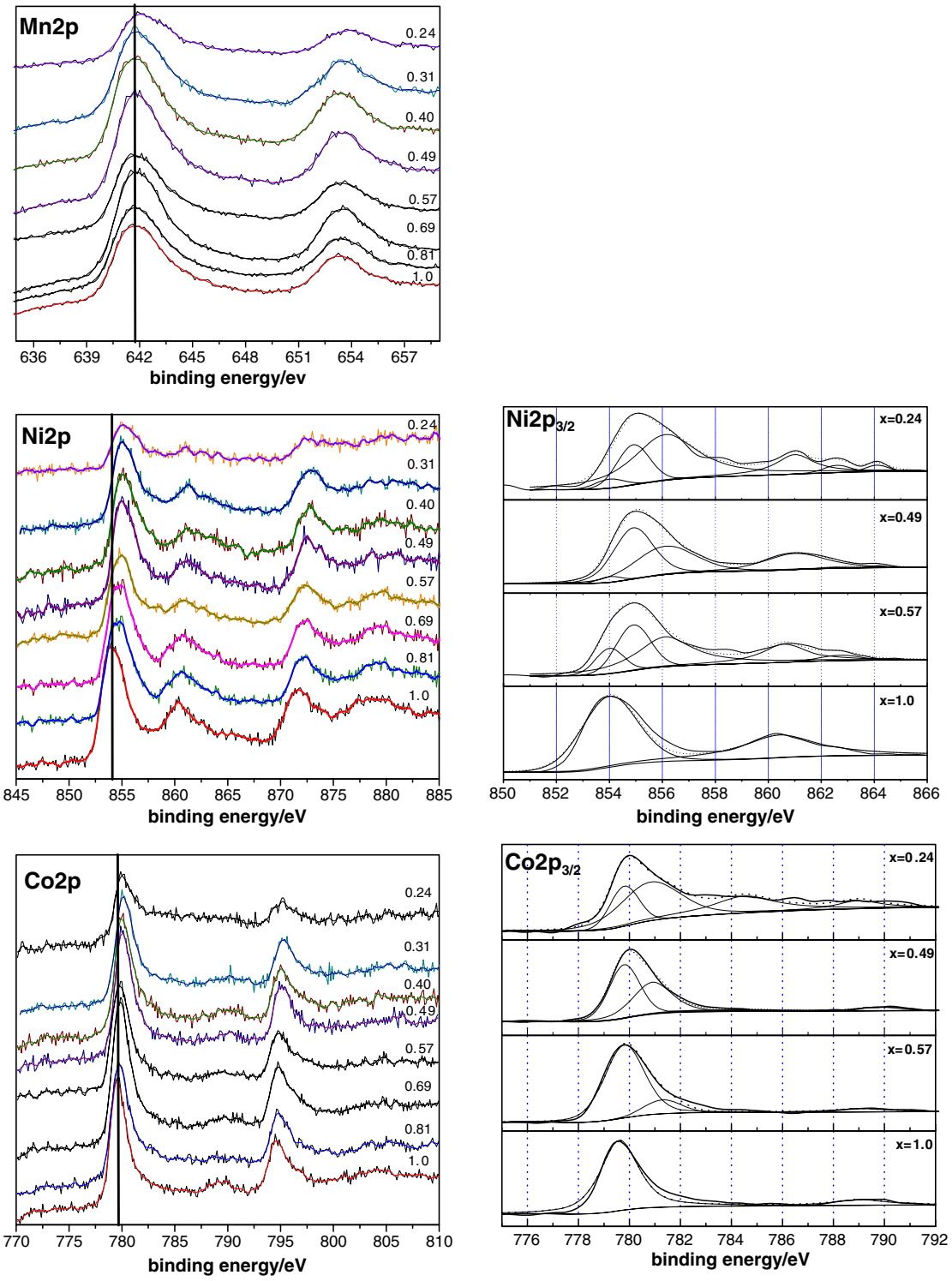

Fig. 5. Mn2p, Ni2p and Co2p XPS spectra of $Li_xNi_{1/3}Mn_{1/3}Co_{1/3}O_2$ ($0<x\leq 1$) cathode material; the curve fitting for Ni2p ($x=0.24$, 0.49, 1.0) and Co2p ($x=0.24$, 0.49, 0.57, 1.0) was also presented at the right of the graph for comparison.

(110) and (108) crystal planes, it is found that the (003) and (108) diffraction peaks slightly shift towards the lower angles when x changes from 1.0 to 0.49, but it slightly shifts back to higher angles when x changes from 0.4 to 0.24. On the other hand, the (110) peak increases firstly and then changes little when $x\leq 0.49$. As explained in our previous paper [16], the shift of (003) peak corresponds to the reciprocating changes of c axis (interslab distance), while the shift of (110) peak corresponds to the changes of a axis. That is to say, crystal lattice expanded firstly and then contracted in c axis direction, while it kept contracted to a constant value in a axis and then maintains it. Rietveld refinement results (Table 1) also prove

the structure changes simultaneously. ~ 3% of the Ni migrated from the 3b to 3a site, while the Co and Mn remained on the 3b site. Therefore, we could explain the above observation as follows: when lithium content is still higher, two O-layers should contact closely as some of lithium ion is released, thus repulsion between same electric charges makes the lattice slightly expand in *c* axis. When more lithium ions are released ($x \leq 0.49$), many vacancies formed and become main state of Li layer; the lattice structure collapses to some extent and it could be imagined that the crystal lattice contracts in *c* axis at that time. In addition, because of the average oxidation state of Co, Ni and Mn increase with the decrease of *x*, charge repulsion becomes weaker in Li layer and stronger in transition metal layer. Both two different effects make the lattice contracts in *a* axis firstly and then maintains it at a suitable level.

After checking the (003) peak carefully, the peak only slightly shifts in the whole range of $0.24 \leq x \leq 1$. There is no new peak observed in the XRD patterns, indicating that no new phase appears. Although the lattice expands and contracts, it maintains O3-type single phase all the time, which is different from higher Ni content systems such as $LiNi_{0.75}Mn_{0.25}O_2$ [23] and $LiNi_{0.8}Co_{0.2}O_2$ [16]. Some researches have reported that a new phase O3' for delithiated materials appear in these systems ($x=0.5$ for $LiNi_{0.8}Co_{0.2}O_2$ and $x=0.3$ for $LiNi_{0.75}Mn_{0.25}O_2$). In contrast, $LiNi_{1/3}Co_{1/3}Mn_{1/3}O_2$ exhibits better crystal structural stability. Besides, the percentage of Ni ion at the 3a site fluctuates about 3% without obvious change. It is possible for the presence of significant amount of an electrochemically inactive Mn^{4+} ion in this system, which may play an important role in stabilization of the crystal structure of the materials.

Fig. 4 shows the result of iodometric titration experiment. Supposed that the oxygen species were stable, average oxidation state of the three transition metals should keep a nearly linear increase as lithium content decrease. This change is necessary to balance the electric charge in the materials. Certainly, lattice oxygen will become more active after deintercalation of lithium ions, but it would not affect the changing trend of oxidation state of the metal ions.

In order to compare and determine the oxidation states of metal ions and cationic distribution, XPS technique was used to characterize the delithiated materials.

The Ni2p, Co2p and Mn2p XPS spectra for $LiNi_{1/3}Co_{1/3}Mn_{1/3}O_2$ are shown in Fig. 5. It is found that Mn2p (Fig. 5) main peak is located at 641.1 eV, similar to the binding energy in β-MnO_2 [24]. The slight shift of peak for $x=0.31$ and $x=0.24$ arise from the changes in the Mn local environment, not from the changes of the oxidation state upon charging process [12]. Thus Mn ion should have stable oxidation state in this system, holding +4 for $0.24 \leq x \leq 1$.

Different from Mn ions, binding energy (BE) of Ni2p (Fig. 5) changes obviously. When $x=1$, the spectrum shows the main peak ($Ni2p_{3/2}$) at 854.0 eV which can be attributed to Ni^{2+}. With lithium ion released, the BE value of the main peak keep rising. Characteristic satellite peak of $Ni2p^{2+}_{3/2}$, which locates at 861.0 eV also decrease during the process. They all imply that oxidation state of Ni ions keep increasing in the deintercalation process. Pay attention to the curve fitting for 850–865 eV, intensity of main peak (854.0 eV) for Ni^{2+} ions goes weaker as Li^+ is released. Though Ni^{2+} ions leave about 18.6% for $x=0.57$ according to the area percentage (Table 2), the peak for Ni^{2+} ions is nearly invisible when *x* decrease to 0.49. At the same time, the main peaks for Ni^{3+} (854.9 eV) emerge and become stronger [25,26] at this *x* range. That is to say, changes of $Ni^{2+} \rightarrow Ni^{3+}$ is almost completed at that time, +3 becomes the main value for $x=0.57$ and 0.49. When $x \leq 0.49$, the situation is different. As the main state of Ni ion, most Ni^{3+} ions continue to lose electrons and raise their oxidation state as lithium ion is released. Percentage of Ni^{4+} (the main peak located at 856.1 eV) increases to 72.8% for $x=0.24$, now +4 becomes the main oxidation state. It is obvious that some of the Ni^{3+} ions change to Ni^{4+} ions at the beginning of the deintercalation process of Li^+ ions, but it is still not the main process at that time. In one word, $Ni^{2+} \rightarrow Ni^{3+} \rightarrow Ni^{4+}$ occurred in the system, but $Ni^{3+} \rightarrow Ni^{4+}$ only occurred at higher voltage.

It should be noted that Ni^{3+} is an ion with Jahn-Teller effect. When it becomes the main state of Ni ions in the $Li_xNi_{1/3}Co_{1/3}Mn_{1/3}O_2$ system, the $[NiO_6]$-octahedron will be distorted because of the Jahn-Taller effect. DOS obtained by calculation has also proved this phenomenon [7,27].

Fig. 5 shows XPS patterns of Co2p of the materials with different intercalation states. At the beginning of deintercalation process, few changes can be observed in these spectra. When $x=0.49$, the main peak begins to shift to higher binding energy, indicating that oxidation state of Co ion starts to increase. Curve fitting of the peak at 775–793 eV shows that only two peaks can be separated for $x=1$. One with BE value of 789.0 eV is a characteristic satellite peak of Co^{3+}, the other with BE value of 779.5 eV is the main peak for Co^{3+} ion. Thus +3 is the main oxidation state of Co ions in the initial sample. Then the other two peaks appear in the curves when $x=0.57$ which could be attributed to the main peak and characteristic satellite peak for the Co^{4+} with BE values of 780.9 eV and 784.5 eV, but they are not distinctive. According to the area percentage, only 10.8% of Co ions changed to +4 values. That is to say, when $x \leq 0.57$, Co ion maintain +3, but also shows the trend of changing to +4 [26,28] at higher *x* value. When $x=0.49$, the relative intensity of main peak of Co^{3+}/Co^{4+} evidently decreases, characteristic satellite peak of the Co^{4+} is as high as that of Co^{3+} and the percentage of Co^{4+} increases to 38.1%. When $x=0.24$, 69.9% cobalt ions are Co^{4+}, the characteristic satellite peak of Co^{3+} disappear simultaneously and +4 becomes the main oxidation state of Co ions. Thus we consider that Co ions keep stability relatively at the beginning of charge process, but lost electron to increase its oxidation state to +4 after 43% of lithium ions is

Table 2
The area percentages of main peaks of different oxidation states for Ni and Co ions when $x=0.24$, 0.49, 0.57, 1.0 in $Li_xNi_{1/3}Mn_{1/3}Co_{1/3}O_2$ cathode materials in XPS spectra

x	Ni2+	Ni3+	Ni4+	Co3+	Co4+
1	100%	–	–	100%	–
0.57	18.6%	47.5%	33.9%	89.2%	10.8%
0.49	3.1%	52.2%	44.7%	61.9%	38.1%
0.24	4.5%	22.7%	72.8%	30.1%	69.9%

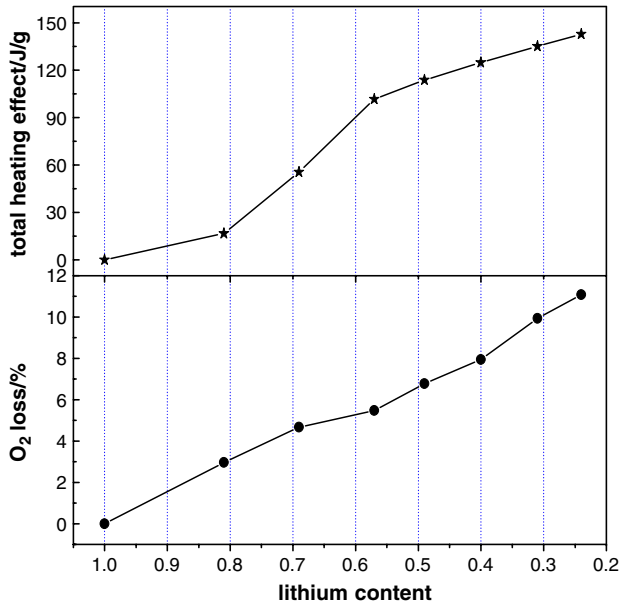

Fig. 6. Percentage of TG loss and total heating effect of $Li_xNi_{1/3}Mn_{1/3}Co_{1/3}O_2$ ($0<x\leq 1$) cathode material after heating at 900 °C.

released. In other words, different from that of nickel ions, oxidation states of cobalt ions only change at higher voltage.

3.3. Thermal stability of the materials and correlation to changes of the oxygen species

In order to study the thermal stability and changes of oxygen species in the delithiation process of Li ions, TPD-MS [17] and TG-DSC technique were used for this purpose. Both two kinds of the experiments were carried out under a nitrogen stream, with a heating rate of 10 °C/min.

Fig. 6 shows the percentage of weight loss and total exothermic effects of the delithiated samples between room temperature and 900 °C. It is obvious that the total exothermic heat increases with the release of the lithium ion, e.g. from 0 J/g for $x=1$ in $Li_xNi_{1/3}Co_{1/3}Mn_{1/3}O_2$ to 142.9 J/g for $x=0.24$. It is more sensitive to temperature for delithiated materials, which will affect its thermal stability. At the same time, the weight loss of the sample is only 2.97% for $x=0.81$, but increases to 11.08% for $x=0.24$. To investigate the origins for these weight loss and exothermic effect, TPD-MS experiment was carried out. We collected the signal of H_2O, O_2 and CO_2 in the measurement simultaneously, which might exist in the system or be produced in the heating process, but only the changes of oxygen species, i.e. oxygen molecule, were observed. The results indicate that with the increase of temperature, evolution of oxygen from the materials may contribute to the exothermic effect and weight loss of the delithiated $Li_xNi_{1/3}Co_{1/3}Mn_{1/3}O_2$. The chemical reaction that occurred could be proposed as follows:

$$Li_xNi_{1/3}Mn_{1/3}Co_{1/3}O_2 \xrightarrow{\Delta} Li_xNi_{1/3}Mn_{1/3}Co_{1/3}O_{2-y} + 1/2yO_2$$

Fig. 7 shows a comparison of the TG curves and the O_2-TPD-MS spectra for $x=0.49$ and $x=0.24$. It can be seen clearly that only a big peak appears in the differential TG (DTG) curve at 565 °C for $x=0.49$, the onset temperature for the weight-loss peak is the same as that of the peak in O_2-TPD-MS spectra, which corresponded with the oxygen evolution from the materials. Thus the weight loss can be attributed to oxygen evolution from the sample. When $x=0.24$, two peaks shown in the differential TG curve are located at 330 °C and 490 °C. The onset temperature is also the same as that of the peak in O_2-TPD-MS spectra. It indicates that more oxygen gas evolved at lower temperature when more lithium were removed (deintercalated) from the initial materials, i.e. when more lithium ions were released from the cathode materials during charging process, evolution of oxygen from the materials will become easier.

Fig. 8 shows O_2-TPD-MS results of delithiated $Li_xNi_{1/3}Co_{1/3}Mn_{1/3}O_2$ within the temperature range of 100–800 °C, three sets of peaks located at different temperature are observed, which represent three different forms of oxygen species. It is obvious that the phenomenon of oxygen evolution only occur at higher temperature regions at the lower deintercalated state ($x\geq 0.49$). Then more oxygen evolved from the materials with lower onset temperature as more lithium ions deintercalated. In addition, the peak located at the temperature of 240–350 °C

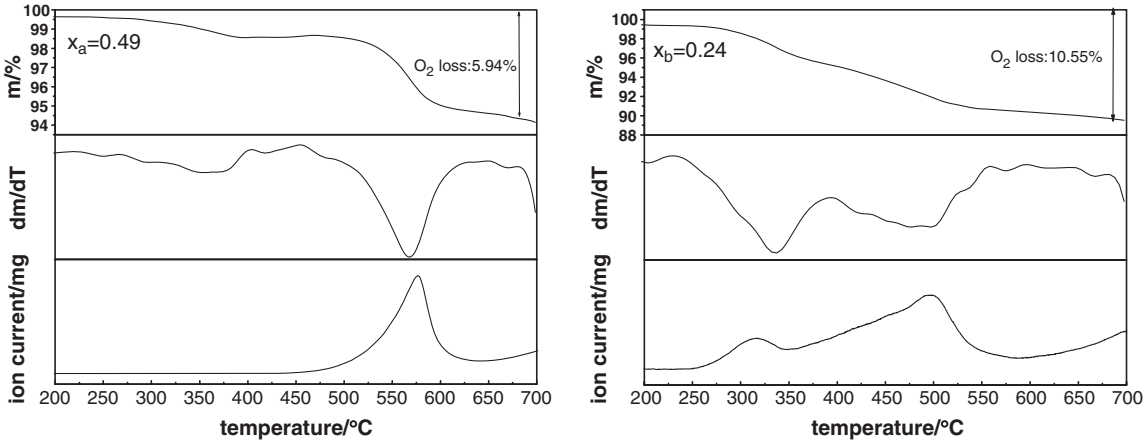

Fig. 7. A comparison of O_2-TPD-MS and TG curves of delithiated $Li_xNi_{1/3}Mn_{1/3}Co_{1/3}O_2$ ($x_a=0.49$, $x_b=0.24$) cathode materials.

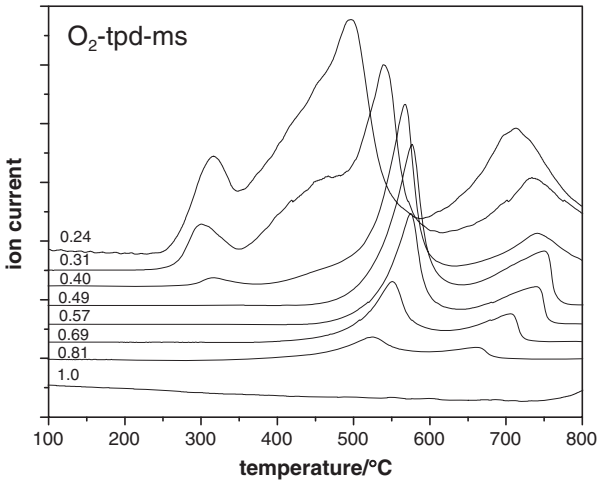

Fig. 8. O_2-TPD-MS patterns of $Li_xNi_{1/3}Co_{1/3}Mn_{1/3}O_2$ ($0<x\leq 1$) in the range of 100–800 °C.

should correspond to physical absorbed oxygen species (marked as α-O) [29], the peak at temperature of 600–800 °C should correspond to lattice oxygen (marked as β-O), and the peak in 350–600 °C should correspond to chemical absorbed partially charged oxygen species $O^{\delta-}$ (including O_2^-, O^-, O_2^{2-}, marked as χ-O) [30]. We consider that the chemical absorbed oxygen exists as a negative ion with less charge than O^{2-}, therefore it should be more active than normal lattice oxygen species. Different from physical absorbed oxygen species, it does not leave easily the lattice position in some cases, but its activity is much higher than lattice oxygen.

It should be mentioned that the onset temperature of oxygen evolution peak of β-O species changes from 522.6 °C for $x=0.81$ to 575.5 °C for $x=0.49$, the temperature rises about 53 °C. At same time, the peaks of χ-O shift from 661.7 °C for $x=0.81$ to 750.0 °C for $x=0.49$, the temperature rises about 88 °C. It seems quite difficult to understand these results, but if we consider that the evolution of both chemical absorbed oxygen and lattice oxygen are dependent on strength of M–O bond, it is easier to understand the phenomenon, i.e. the

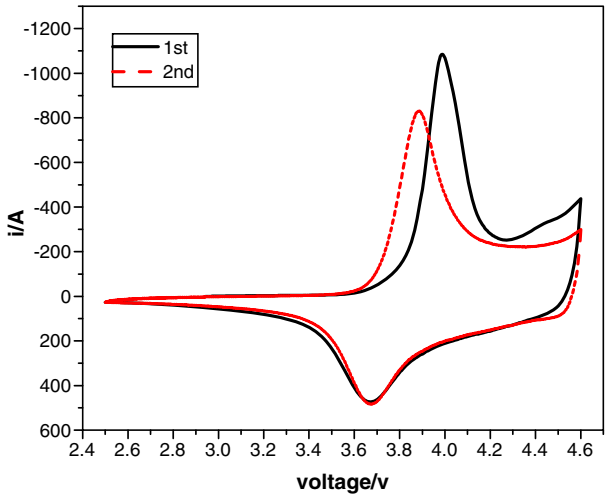

Fig. 9. The CV curve of $LiNi_{1/3}Mn_{1/3}Co_{1/3}O_2$ cathode material.

Table 3
Corresponding relation between charge voltage and lithium ion content

Lithium ion content	0.8	0.6	0.5	0.4	0.2
Charge voltage (V)	3.77	4.09	4.31	4.42	4.62

increased oxidation states of M ions might increase the strength of the M–O bonds. According to the previous analysis about oxidation state of transition metals, Ni^{2+} ions will increase its valence state (they will be oxidized further from +2 to +3 and +4 as more lithium ions deintercalate from the materials), thus the bond energy of Ni–O strengthens and needs more energy (i.e. at higher temperature) to break it in the same range of x. Furthermore, the Rietveld refinement results have also shown that the c/a ratio increases with the decrease of lithium content for $x\geq 0.49$. Ionic diffusion and rearrangement of crystal lattice may partially occur in the samples, and contribute to strengthen the stability of crystal structure. That is the reason why the temperature for the evolution of both χ-O and β-O increases in this range despite more active oxygen obtained.

But later on, when more lithium ions were extracted from the materials (i.e. $x\leq 0.49$), the peak appears at lower temperature region. The amount of α-O keeps increasing with more lithium ions deintercalated. TG experiment has also demonstrated that the amount of active oxygen keeps increasing as the lithium content decreases. Thus a great deal of active oxygen exists in the sample. At the same time, some active oxygen species continue to lose electron, forming O_2 molecule to balance electric charge, which will partly leave from the crystal lattice and settle at the sample's surface through physical adsorptive force, such as van der Waals' force. As the result of formation of weaker chemical bond, α-O may be released at lower temperature. Then the attracting force in Li–O layer and M–O layer is unbalanced. It will also result in not only releasing α-O, but also χ-O and β-O.

According to the analysis of O_2-TPD-MS, the transformation process of oxygen species into oxygen gas could be proposed as follows: $2O^{2-}{}_{(lattice)}\rightarrow\{2O^-, O_2^{2-}, O_2^-\}_{(chemical\ absorbed)}\rightarrow O_{2(physical\ absorbed)}\rightarrow O_{2(gas)}$. When $x>0.49$, under suitable temperature conditions, χ-O and β-O are the main forms of oxygen species. For chemical absorbed oxygen species, although their valence states are not −2 values, most of them are located at lattice position in the materials. But after lithium content is less than 49%, some part of oxygen species will leave lattice, and turn into physical absorbed molecular oxygen species, which mainly locates at material surface. If this process happens, it could result in further evolution of oxygen gas from the surface.

3.4. Further electrochemical experiments of the material

Fig. 9 shows a typical cyclic voltammetric curve of $Li_xNi_{1/3}Co_{1/3}Mn_{1/3}O_2$ material during the first two cycles. It is noticeable

Table 4
The charging efficiency of $LiNi_{1/3}Mn_{1/3}Co_{1/3}O_2$ material when it charges/discharges between different voltage ranges during the first cycle

	3 – 4.0 V	3 – 4.1 V	3 – 4.2 V	3 – 4.3 V	3 – 4.4 V	3 – 4.5 V	3 – 4.6 V
Efficiency (%)	86.3	87.1	88.0	79.8	74.4	70.7	69.3

that two oxidation peaks were observed in the first cycle. The first one located at 3.8 V with the onset potential at about 3.6 V is quite reversible with a corresponding reduction peak at 3.7 V. The second oxidation shoulder peak could appear at about 4.4 V. But there is no obvious corresponding reduction peak for this process, indicating the irreversibility of this redox reaction. It is well known that the potential of the electrode is determined by the lithium contents intercalated in the insertion electrodes according to a Nernst equation, i.e. quantitative lithium ions are released at a determined charging voltage in a stable battery system. Table 3 shows a relationship between charging voltage and lithium ion content in the materials. For example, more than 50% (~ 0.49) of lithium ion has been released at 4.3 V. According to XPS results, with the change of $Ni^{3+}\rightarrow Ni^{4+}$, Co^{3+} begins to increase its oxidation state to +4. Both of the above changes may partially contribute to the second oxidation peak in CV curve. In order to understand the phenomenon deeply, we charged and discharged a set of CR2025 coin cells at different voltage range (the charging efficiency of the material between different voltage range are listed in Table 4, the end of discharging voltage were all set at 3.0 V). It is found that the efficiency of first cycle changes little when charging voltage is set at lower than 4.3 V ($x \leq 0.49$), indicating a reversible reaction of electrochemical process. However, when the charging potential is higher than 4.3 V, the charging efficiency begins to decrease rapidly. In other words, these irreversible structural changes of delithiated materials for $x \leq 0.49$ will partially affect the intercalation process of lithium ion when discharging, and cause irreversible capacity loss during the first cycle.

In addition, at the high charging voltage of 4.6 V, decomposition reaction of the electrolytes that may also contribute to the second peak in CV curve is inevitable [17]. This kind of reaction should also practically result in some irreversible capacity loss to $LiNi_{1/3}Co_{1/3}Mn_{1/3}O_2$ material. We will investigate about it in our future work.

4. Conclusion

Comparing with some commercialized cathode materials (e.g. $LiCoO_2$, $LiNi_{0.8}Co_{0.2}O_2$), $LiNi_{1/3}Co_{1/3}Mn_{1/3}O_2$ prepared by sol–gel method has shown excellent electrochemical performance as a cathode material in lithium ion battery, especially at high charging voltage. The material is able to keep its single phase during chemical delithiation process as demonstrated by our ex-situ XRD results.

But oxidation states of Ni and Co increase to +4 when charging the material to high voltage ($V \geq 4.3$ V), i.e. $Ni^{3+}\rightarrow Ni^{4+}$ and $Co^{3+}\rightarrow Co^{4+}$. These changes that happened at the first cycle are partly irreversible, which may cause negative effects on the electrochemical performance of material. Simultaneously, active oxygen species such as O_2^-, O^-, O_2^{2-} will lose some electrons to form O_2, or immigrate to the surface of material at higher charging voltage. Parts of them are even released from the delithiated materials. These irreversible changes also break the balance of charge and species in the original materials, affecting insertion of lithium ions into delithiated materials when it is discharged.

Certainly, most of the results obtained here is based on the chemically delithiated system which ignored the reactions of electrolytes of the practical electrochemical system. However, it is no doubt that our results presented here will be helpful to understand the structural changes of the materials and chemical activity of the lattice oxygen species during the electrochemical delithiation process in $LiNi_{1/3}Co_{1/3}Mn_{1/3}O_2$ cathode materials.

Acknowledgements

We are grateful for the financial support of National Natural Science Foundation of China (NNSFC, Grant Nos. 29925310, 20433060, 20473068).

References

[1] T. Ohzuku, Y. Makimura, Chem. Lett. 7 (2001) 642.
[2] N. Yabuuchi, T. Okzuku, J. Power Sources 119–121 (2003) 171.
[3] I. Belharouak, Y.-K. Sun, J. Liu, K. Amine, J. Power Sources 123 (2003) 247.
[4] K.M. Shaju, G.V. Subba Rao, B.V.R. Chowdari, Electrochim. Acta 48 (2002) 145.
[5] M.-H. Lee, Y.-J. Kang, S.-T. Myung, Y.-K. Sun, Electrochim. Acta 50 (2004) 939.
[6] J.-M. Kim, H.-K. Chung, Electrochim. Acta 49 (2004) 937.
[7] B.J. Hwang, Y.W. Tsai, D. Carlier, G. Ceder, Chem. Mater. 15 (2003) 3676.
[8] S.H. Park, C.S. Yoon, S.G. Kang, H.-S. Kim, S.-I. Moon, Y.-K. Sun, Electrochim. Acta 49 (2004) 557.
[9] D. Li, T. Muta, L. Zhang, M. Yoshio, H. Noguchi, J. Power Sources 132 (2004) 150.
[10] Y. Koyama, I. Tanaka, H. Adachi, Y. Makimura, T. Ohzuku, J. Power Sources 119–121 (2003) 644.
[11] N. Yabuuchi, Y. Koyama, N. Nakayama, T. Ohzuku, J. Electrochem. Soc. 152 (7) (2005) A1434.
[12] Y.M. Tsai, B.J. Hwang, G. Ceder, H.S. Sheu, D.G. Liu, J.F. Lee, Chem. Mater. 17 (2005) 3191.
[13] M.G. Kim, H.J. Shin, J.H. Kim, S.H. Park, Y.K. Sun, J. Electrochem. Soc. 152 (7) (2005) A1320.
[14] G.H. Kim, J.H. Kim, S.T. Myung, C.S. Yoon, Y.K. Sun, J. Electrochem. Soc. 152 (9) (2005) A1707.
[15] J. Choi, A. Manthiram, Electrochem. Solid-State Lett. 7 (10) (2004) A365.
[16] H.S. Liu, J. Li, Z.R. Zhang, Z.L. Gong, Y. Yang, Electrochim. Acta 49 (2004) 1151.
[17] Z.R. Zhang, Z.L. Gong, Y. Yang, J. Phys. Chem., B 108 (45) (2004) 17546.
[18] H.S. Liu, J. Li, Z.R. Zhang, Z.L. Gong, Y. Yang, J. Solid State Electrochem. 7 (2003) 456.
[19] S. Venkatraman, Y. Shin, A. Manthiram, Electrochem. Solid-State Lett. 6 (1) (2003) A9.
[20] Y. Takahashi, J. Akimoto, Y. Gotoh, K. Kawaguchi, S. Mizuta, J. Solid State Chem. 160 (2001) 178.
[21] R.V. Chebiam, F. Prado, A. Manthiram, J. Electrochem. Soc. 148 (1) (2001) A49.
[22] Z.H. Lu, L.Y. Beaulieu, R.V. Donaberger, C.L. Thomas, J.R. Dahn, J. Electrochem. Soc. 149 (6) (2002) A778.
[23] S. Venkatraman, A. Manthiram, Chem. Mater. 15 (2003) 5003.
[24] Y.C. Sun, C.Y. Ouyang, Z.X. Wang, J. Huang, L.Q. Chen, J. Electrochem. Soc. 151 (4) (2004) A504.
[25] K.M. Shaju, K.V. Ramanujachary, S.E. Lofland, G.V. Sunna Rao, B.V.R. Chowdari, J. Mater. Chem. 13 (2003) 2633.
[26] J.F. Marco, J. Ramon Gancedo, M. Gracia, J.L. Gautier, E.I. Rios, H.M. Palmer, C. Greaves, F. Berry, J. Mater. Chem. 11 (2001) 3087.
[27] Y. Koyama, N. Yabuuchi, I. Tanaka, H. Adachi, T. Ohzuku, J. Electrochem. Soc. 151 (1) (2004) A1545.
[28] J.C. Dupin, D. Gonbeau, H. Benqlilou-Moudden, Ph. Vinatier, A. Levasseur, Thin Solid Films 384 (2001) 23.
[29] Z.P. Shao, W.S. Yang, Y. Cong, H. Dong, J.H. Tong, G.X. Xiong, J. Membr. Sci. 172 (2000) 177.
[30] Z. Zhao, X.G. Yang, Y. Wu, Appl. Catal., B Environ. 8 (1996) 281.